Accurate electron affinity of Co and fine-structure splittings of Co^- via slow-electron velocity-map imaging

Xiaolin Chen[1] and Chuangang Ning[1,2,*]

[1]*Department of Physics, State Key Laboratory of Low-Dimensional Quantum Physics, Tsinghua University, Beijing 10084, China*

[2]*Collaborative Innovation Center of Quantum Matter, Beijing, China*

(Received 23 March 2016; published 12 May 2016)

The high-resolution photoelectron spectra of Co^- were obtained via the slow-electron velocity-map imaging method. The electron affinity of cobalt element was determined to be 5341.45(37) cm^{-1} or 662.256(46) meV. The fine structure of Co^- was well resolved. The fine-structure intervals $Co^-(^3F_4) - Co^-(^3F_3)$ and $Co^-(^3F_4) - Co^-(^3F_2)$ were found to be 920.9(6) cm^{-1} and 1550.3(9) cm^{-1}, respectively. The accuracy was improved by a factor of more than ten with respect to the previous laser photodetachment threshold measurement.

DOI: 10.1103/PhysRevA.93.052508

I. INTRODUCTION

Negative ions are unique species and play important roles in many branches of physics and chemistry, such as astrophysics [1–3], plasma physics, gas-phase ion chemistry, environment chemistry, and many other fields [4]. Photoelectron spectroscopy of negative ions can determine the electron affinities (EAs), an important parameter that determines the structure of anions. The measured accuracy of EAs of atoms has steadily improved over the past 46 years [5–7]. However, the uncertainty of EAs for many transition elements still remains around 10 meV due to the low cross section of p-wave threshold photodetachment and the complicated electronic structures [7].

The measured accuracy of the laser photodetachment electron spectroscopy (LPES) is limited by the energy resolution of the electron spectrometer, which is typically around 10 meV [8–10]. On the other hand, accuracies of the laser photodetachment threshold (LPT) method range from 0.1 to 0.001 meV, as they are often only limited by the laser bandwidth [6,11–14]. By using the LPT method with a tunable infrared laser, Haugen and co-workers reported many precise EA values [14], such as B [15], Al [16], Co [17], and Ru [18]. Recently, Blondel and co-workers reported a pioneering method based on the laser photodetachment microscopy (LPM) method [19]. The uncertainties of the EA values for O [20], OH [21], C [22], and Ge [23] have gone down to sub-μeV level via LPM. However, the low cross section of p-wave threshold photodetachment [24] and the complicated electronic structures pose a significant restriction on the application of LPT and LPM methods for transition elements. The typical photoelectron kinetic energy of LPM is lower than 1 cm^{-1}. It would be extremely difficult to apply the LPM method for transition-metal anions. Hence, no LPM measurement for EAs of transition metals has been reported. The LPT has been applied to several transition elements [17,18]. The accuracy of LPT for p-wave photodetachment depends on the threshold behavior. A systematic deviation from the Wigner's threshold law [24] may deteriorate the accuracy of the LPT method, which has been observed in the Ir^- and Pt^- studies [25]. Moreover, the LPT method cannot resolve the congested p-wave photodetachment channels with a separation less than 20 cm^{-1} due to the zero-slope onset at the threshold. Recently, our group demonstrated that the slow-electron velocity-map imaging (SEVI) method can significantly improve the measured accuracy of EAs for transition elements [26,27]. For example, the electron affinity of Nb was measured as 7399.35(50) cm^{-1} via the SEVI method [26]. The accuracy was improved by a factor of more than 400 with respect to the previous measurement [8]. The SEVI technique was previously developed by Neumark and co-workers [28,29]. SEVI has a very impressive energy resolution for electrons with low kinetic energy [26,30–34]. In this article, we report an improved EA measurement of Co and the fine-structure splitting of Co^- via the SEVI method.

Cobalt is one of the important constituents in production of certain high-performance alloys and catalysts. The negative ion of cobalt has been the subject of substantial experimental and theoretical work [17,35–38]. The ground-state configuration of Co^- is $(3d^8\,4s^2)\ ^3F_4$, while the ground-state configuration of Co is $(3d^7\,4s^2)\ ^4F_{9/2}$. Utilizing LPES combined with a fixed-frequency 488-nm laser, Corderman *et al.* [35] measured the EA of Co to be 662(10) meV, and the $J = 4-3$ and $J = 3-2$ splittings were extrapolated as 910(50) and 650(50) cm^{-1}. Note that 1 eV = 8065.544 005(50) cm^{-1}, as recommended by 2014 CODATA [39]. Later, an improved value 662(3) meV for EA(Co) was reported by using a cold flowing afterglow ion source [36]. Recently, Scheer *et al.* [17] measured EA(Co) to be 663.3(6) meV or 5349.9(48) cm^{-1} via the LPT method. In addition, the fine-structure splitting of $J = 4-3$ was measured as 875(15) cm^{-1}. The $J = 4-2$ splitting was not reported in the work. The aim of the present paper is to improve the accuracy of EA(Co) to sub-cm^{-1} level and to measure $J = 4-2$ splitting. In addition, it is worthy to compare the different techniques for measuring EAs of transition elements and fine structures of negative transition element ions.

II. EXPERIMENTAL SETUP

Figure 1 shows the schematic view of the experimental setup used in the present work [26]. In brief, the apparatus includes three major sections: a laser ablation ion source, a Wiley-Mclaren type time-of-flight (TOF) mass spectrometer

*ningcg@tsinghua.edu.cn

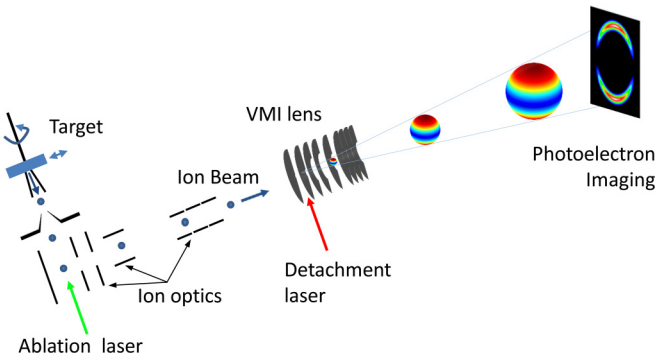

FIG. 1. Schematic diagram of the experimental setup. A mass gate and a rotatable ion detector in the front of the VMI lens are not shown. See text for details.

[40], and a photoelectron velocity-map imaging (VMI) system. The negative ion Co^- is generated using a pulsed laser ablation source operated at 20-Hz repetition rate. The second-harmonic output of a Nd:YAG laser (∼15 mJ/pulse) is focused onto a continually rotating and translating Co metal disk. An in-line sodium oven is used to introduce the sodium vapor to get rid of the trace oxygen and water contamination in the source cell and in the carrier helium gas. The sodium oven is essential for producing anions of the transition metals which oxidize readily [26]. After skimmer, the anions are extracted perpendicularly into a TOF mass spectrometer. The anionic species are accelerated to 900 eV by a high-voltage pulse and then are guided by a set of deflectors and focused by a set of einzel lenses into a 1.4-m-long TOF tube. The mass resolution ($M/\Delta M$) of the current design is 300 for $M \sim 100$. The target ion species are selected by a mass gate and detected by an in-line microchannel plate detector. The ion detector is rotatable. It can be moved out of the ion path during the subsequent photoelectron imaging measurement. The selected anions enter the velocity-map imaging lens system through a 6-mm-diameter aperture on the repeller plate of the VMI lens. The VMI lens system is similar to the design from Ref. [32], which was originally used by the ion imaging experiment [41,42]. Then, the selected ions are perpendicularly crossed by the detachment laser beam in the interaction zone. The laser beam size is limited to 3 mm in diameter by passing through a set of apertures. The photodetachment laser is from a Spectra-Physics dye laser system (40−920 nm, linewidth 0.06 cm^{-1} at 625 nm) pumped by a Quanta-Ray Pro 290 Nd:YAG laser (20 Hz, 1000 mJ/pulse at 1064 nm). The photon energy ($h\nu$) is further measured by a HighFinesse WS6-600 wavelength meter with an accuracy of 0.02 cm^{-1}. The detached photoelectrons are projected onto a phosphor screen behind a set of microchannel plates and recorded by a CCD camera. A real-time intensity-weighted centroid program is used to determine the hitting position of each photoelectron. Typically, each photoelectron imaging is an accumulated result of 50 000−200 000 laser shots. The photoelectron spectrum is then generated by an inverse-Abel transformation of the raw photoelectron imaging [43].

To achieve the best energy resolution, it is required to carefully adjust the voltages of the VMI lens, the laser-anion-beam overlap, and the timing sequence controlled by an eight-channel pulse or delay generator. The iodine anion I^- is used as the test sample for optimizing the imaging system, because a high photoelectron count rate is readily achieved due to the s-wave photodetachment around its threshold. Moreover, the photoelectron image usually has a slight distortion. As a result, a circle becomes an oval. The distortion can be easily fixed by a linear transformation of the coordinates of photoelectrons if the imaging system is running the real-time photoelectron counting mode. One feature of VMI is that the imaging voltage can be adjusted according to the specific requirement of an experiment. A full spectrum can be obtained at a higher voltage, and the fine structures of the spectrum can be zoomed in at a lower voltage. The imaging voltages that we often use are −40 V, −150 V, and −650 V. At the imaging voltage −40 V, the energy resolution we obtained is 0.56 cm^{-1} for $E_k = 1.38\ cm^{-1}$, and 5.1 cm^{-1} for $E_k = 93.6\ cm^{-1}$. With the imaging voltage −150 V, the energy resolution is 3.3 cm^{-1} for $E_k = 25\ cm^{-1}$, which is the typical E_k for the present EA measurement. At the imaging voltage −650 V, the best relative energy resolution we obtained is 2% for $E_k = 3500\ cm^{-1}$.

III. RESULTS AND DISCUSSION

Figure 2 shows the photoelectron energy spectra of Co^- at the photodetachment photon energy $h\nu = 12\,495.68$ and $12\,982.45\ cm^{-1}$ with the imaging voltage −650 V. There are eight sharp peaks. According to the $9j$ calculations and the previous work by Scheer *et al.* [17], the eight peaks are related to ten transitions, which were labeled as $a-j$. The photoelectron image in the inset clearly shows parallel transitions as expected due to the p-wave photodetachment. The related transitions are illustrated in Fig. 3. The vertical spikes in Fig. 2 are the theoretical simulation at the ion temperature 800 K according to the assignment [17,44]. The calculated intensity has been rescaled according to the Wigner's threshold law $\sigma \propto E_k^{3/2}$ for p-wave detachment. Here σ is the photodetachment cross section. The excellent agreement with the experimental

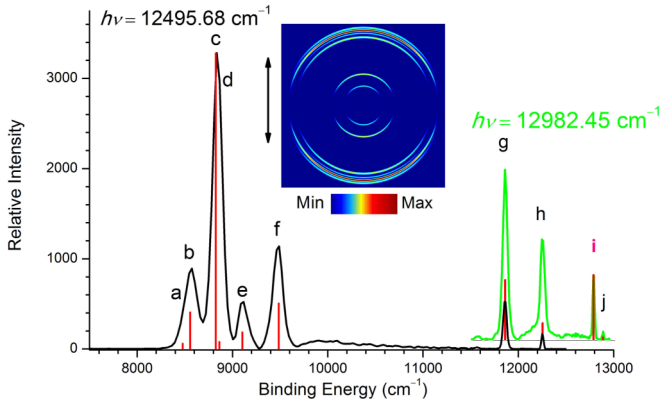

FIG. 2. Photoelectron image and spectrum of Co^- ions obtained with $12\,495.68\ cm^{-1}$ and $12\,982.45\ cm^{-1}$ photons. The double arrow indicates the laser polarization. The vertical red spikes indicate the location and the calculated intensity for the allowed transitions at the temperature 800 K. Peak i is related to the $Co(^2F_{7/2}) \leftarrow Co^-(^3F_4)$ transition, which is used to measure the electron affinity of Co in the present work.

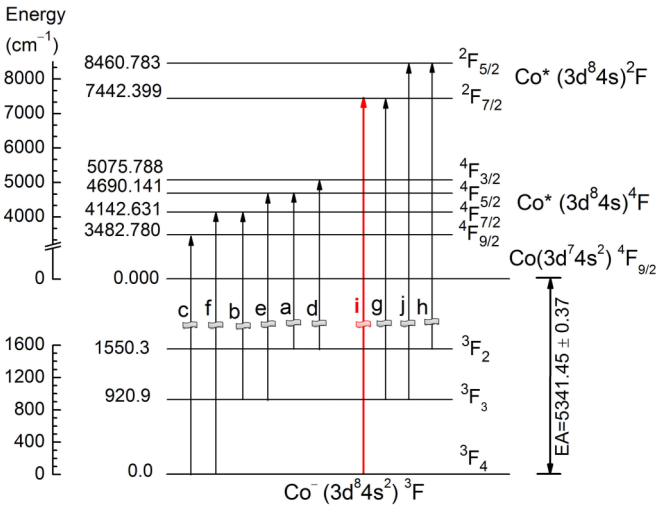

FIG. 3. Energy levels of Co and Co$^-$ related to the present measurement. The ground state of Co is $^4F_{9/2}$. The ground state of Co$^-$ is $^3F_4$. The labels of each transition are the indexes of the observed peaks in Fig. 2. The transition i is used for the electron affinity measurement.

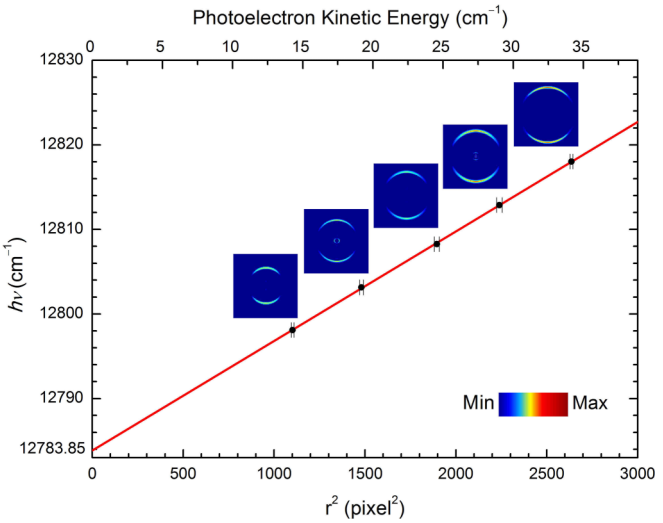

FIG. 4. Energy calibration of the photoelectron velocity-map imaging system. Points with error bars are experimental data of the transition iCo($^2F_{7/2}$) ← Co$^-$($^3F_4$). The solid line is the best linear fitting. The rings above each point are the photoelectron images. The imaging voltage is −150 V.

results confirmed the assignment. Transitions c [Co($^2F_{9/2}$) ← Co$^-$($^3F_4$)], f[Co($^2F_{7/2}$) ← Co$^-$($^3F_4$)], and i[Co($^2F_{7/2}$) ← Co$^-$($^3F_4$)] are photodetachment channels from the ground state of Co$^-$, but only transition i is in the tuning range of our dye laser system. So, transition i was selected as the target channel for the present EA measurement.

To accurately determine EA(Co), the imaging voltage −150 V was used. The energy scale of the VMI system was carefully calibrated for transition i. After inverse-Abel transformation [43], the hitting positions of photoelectrons on the phosphor screen form a circle for an individual transition. The radius r of the circle is proportional to the velocity of photoelectrons v. The radius can be obtained by summing the intensity over all angles and then finding the peak center by a Gaussian function fitting. A series of photoelectron spectra were measured with the photon energy scanned from 12 798 cm^{-1} to 12 818 cm^{-1} with a 5-cm^{-1} step. The measured square of radius (r^2) versus the photon energy $h\nu$ is plotted in Fig. 4. The energy calibration parameters of the linear relation between $h\nu$ and r^2 were determined by a best linear fitting. The binding energy of transition i and its uncertainty were obtained by the procedure. Figure 5 shows the measured binding energy versus the photoelectron kinetic energy. Its mean binding energy is 12 783.85 cm^{-1} with an uncertainty of 0.37 cm^{-1}. The energy level of the neutral Co atom $(3d^8\,4s)\,^2F_{7/2}$ state is 7442.399 cm^{-1} above its ground state [45]. Therefore, EA of Co is determined as 5341.45 ± 0.37 cm^{-1}. The uncertainty 0.37 cm^{-1} has included the contribution of the laser linewidth 0.06 cm^{-1}.

The fine structure of Co$^-$ $(3d^8\,4s^2)\,^3F$ can be derived from the observed transitions i, j, g, and h. A least-squares fitting method based on the covariance algebra was used to find the two energy-level values from the four transitions [46,47]. This is a standard spectroscopic method for finding the energy levels of a quantum system based on a set of measured energy separations. The splittings of Co$^-$($^3F_3$) ← Co$^-$($^3F_4$) and Co$^-$($^3F_2$) ← Co$^-$($^3F_4$) were determined as 920.9(6) and 1550.3(9) cm^{-1}, respectively.

The measured binding energies of related transitions and fine structures of Co$^-$ are summarized in Table I in comparison with the previous works. There is a 1.04-meV difference between our measured EA value 662.256(46) meV and the value 663.3(6) meV measured by Scheer *et al.* [17]. The small discrepancy may be due to the background subtraction. In Fig. 10 of Scheer and co-workers' work [17], a dashed line was plotted to subtract the sloped background. Obviously, their EA value depends on how to subtract the background. Our EA

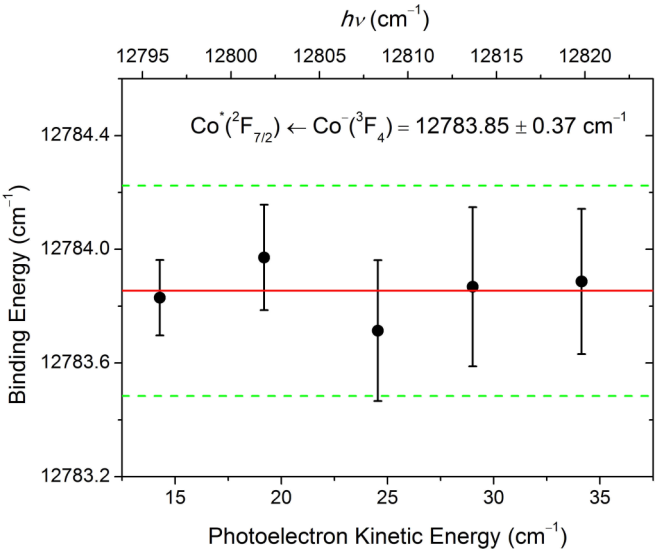

FIG. 5. Binding energy of Co($^2F_{7/2}$) ← Co$^-$($^3F_4$) transition measured as a function of the photoelectron kinetic energy. The dotted lines indicate the ±0.37 cm^{-1} uncertainty.

TABLE I. Measured binding energies and fine structures of Co^- and the electron affinity of Co.

Peak	Levels (Co ← Co^-)	Binding energy (cm^{-1})
a	$^4F_{5/2} \leftarrow {}^3F_2$	
b	$^4F_{7/2} \leftarrow {}^3F_3$	8561(18)
c	$^4F_{9/2} \leftarrow {}^3F_4$	8836(16)
d	$^4F_{3/2} \leftarrow {}^3F_2$	
e	$^4F_{5/2} \leftarrow {}^3F_3$	9105(16)
f	$^4F_{7/2} \leftarrow {}^3F_4$	9471(14)
g	$^4F_{7/2} \leftarrow {}^3F_3$	11863.0(14)
h	$^2F_{5/2} \leftarrow {}^3F_2$	12251.9(17)
i	$\mathbf{^2F_{7/2} \leftarrow {}^3F_4}$	**12783.85(37)**
j	$^2F_{5/2} \leftarrow {}^3F_3$	12881.3(14)

Fine structure of Co^- (cm^{-1})

Levels	Previous work	This work
$^3F_3 \leftarrow {}^3F_4$	875(15) [17]	920.9(6)
	910(50) [35]	
$^3F_2 \leftarrow {}^3F_4$	1560(70) [35][a]	1550.3(9)

Electron affinity of Co

Value	Reference
1450 meV	Cole and Perdew [37] (calculated)
487 meV	Balabanov *et al.* [38] (calculated)
662(10) meV	Corderman *et al.* [35] (measured)
662(3) meV	Leopold and Lineberger [36] (measured)
663.3(6) meV	Scheer *et al.* [17] (measured)
662.256(46) meV or 5341.45(37) cm^{-1}	This work (measured)

[a]Not measured in Ref. [17].

value 662.256(46) meV agrees with the EA value 662(3) meV that was measured by Leopold and Lineberger [36].

The interval between $Co^-(^3F_3)$ and $Co^-(^3F_4)$ was determined to be 920.9(6) cm^{-1}, which is significantly different from the value 875(15) cm^{-1} obtained by Scheer *et al.* [17]. The discrepancy may be due to the poor signal-to-noise ratio of the transition $Co(3d^7\,4s^2)^4F_{9/2} \leftarrow Co^-(^3F_3)$ that they observed. The interval 920.9(6) cm^{-1} agrees with the extrapolated value 910(50) cm^{-1} by Corderman *et al.* [35]. On the theoretical side, the early calculation suggested EA(Co) = 1.45 eV [37]. A more recent calculation reported a value of 0.487 eV [38]. Both studies have significant deviations. The accurate experimental EA(Co) value and the fine structure of Co^- determined in this study could serve as a benchmark for developing more accurate theoretical methods for transition metals.

IV. CONCLUSIONS

In summary, the electron affinity of cobalt element and the fine structure of Co^- have been measured via the slow-electron velocity-map imaging method. The electron affinity of Co was determined to be 5341.45(37) cm^{-1} or 662.256(46) meV. The fine-structure interval $Co^-(^3F_4) - Co^-(^3F_3)$ was determined as 920.9(6) cm^{-1}, and it is 1550.3(9) cm^{-1} for the interval $Co^-(^3F_4) - Co^-(^3F_2)$. The accuracy was improved by a factor of more than 10 with respect to the previous measurement via the laser photodetachment threshold spectroscopy. As shown in this work, the slow-electron velocity-map imaging method has two key features for measuring the electron affinities of transition metals: the high-energy resolution to resolve the congested transitions and the relatively high *p*-wave signal intensity because of the well-above-threshold measurement. These features make it possible to improve the measurement accuracy of EA to sub-cm^{-1} for nearly all transition and lanthanide metal atoms.

ACKNOWLEDGMENTS

This work is supported by National Natural Science Foundation of China (NSFC) (Grant No. 91336104) and Ministry of Science and Technology of China (MOST) (Grant No. 2013CB922004) of the National Key Basic Research Program of China.

[1] J. P. Maier, J. Phys. Chem. A **102**, 3462 (1998).
[2] D. M. Hudgins and L. J. Allamandola, J. Phys. Chem. **99**, 8978 (1995).
[3] S. Petrie, Mon. Not. R. Astron. Soc. **281**, 137 (1996).
[4] J. C. R. Kiracofe, G. S. Tschumper, and H. F. Schaefer III, Chem. Rev. **102**, 231 (2002).
[5] W. C. Lineberger, Annu. Rev. Phys. Chem. **64**, 21 (2013).
[6] W. C. Lineberger and B. W. Woodward, Phys. Rev. Lett. **25**, 424 (1970).
[7] H. Hotop and W. C. Lineberger, J. Phys. Chem. Ref. Data **14**, 731 (1985).
[8] C. S. Feigerle, R. R. Corderman, S. V. Bobashev, and W. C. Lineberger, J. Chem. Phys. **74**, 1580 (1981).
[9] V. T. Davis, J. Thompson, and A. Covington, Nucl. Instrum. Methods Phys. Res., Sect. B **241**, 118 (2005).
[10] J. Felton, M. Ray, and C. C. Jarrold, Phys. Rev. A **89**, 033407 (2014).
[11] D. M. Neumark, K. R. Lykke, T. Andersen, and W. C. Lineberger, Phys. Rev. A **32**, 1890 (1985).
[12] B. Huber, T. M. Miller, P. C. Cosby, H. D. Zeman, R. L. Leon, J. T. Moseley, and J. R. Peterson, Rev. Sci. Instrum. **48**, 1306 (1977).
[13] U. Hefter, R. D. Mead, P. A. Schulz, and W. C. Lineberger, Phys. Rev. A **28**, 1429 (1983).
[14] T. Andersen, H. K. Haugen, and H. Hotop, J. Phys. Chem. Ref. Data **28**, 1511 (1999).
[15] M. Scheer, R. C. Bilodeau, and H. K. Haugen, Phys. Rev. Lett. **80**, 2562 (1998).
[16] M. Scheer, R. C. Bilodeau, J. Thogersen, and H. K. Haugen, Phys. Rev. A **57**, R1493(R) (1998).
[17] M. Scheer, C. A. Brodie, R. C. Bilodeau, and H. K. Haugen, Phys. Rev. A **58**, 2051 (1998).
[18] P. L. Norquist, D. R. Beck, R. C. Bilodeau, M. Scheer, R. A. Srawley, and H. K. Haugen, Phys. Rev. A **59**, 1896 (1999).
[19] C. Blondel, C. Delsart, and F. Dulieu, Phys. Rev. Lett. **77**, 3755 (1996).
[20] C. Blondel, C. Delsart, C. Valli, S. Yiou, M. R. Godefroid, and S. Van Eck, Phys. Rev. A **64**, 052504 (2001).

[21] C. Delsart, F. Goldfarb, and C. Blondel, Phys. Rev. Lett. **89**, 183002 (2002).
[22] D. Bresteau, C. Drag, and C. Blondel, Phys. Rev. A **93**, 013414 (2016).
[23] D. Bresteau, P. Babilotte, C. Drag, and C. Blondel, J. Phys. B: At., Mol. Opt. Phys. **48**, 125001 (2015).
[24] E. P. Wigner, Phys. Rev. **73**, 1002 (1948).
[25] R. C. Bilodeau, M. Scheer, H. K. Haugen, and R. L. Brooks, Phys. Rev. A **61**, 012505 (1999).
[26] Z. H. Luo, X. L. Chen, J. M. Li, and C. G. Ning, Phys. Rev. A **93**, 020501(R) (2016).
[27] X. L. Chen, Z. H. Luo, J. M. Li, and C. G. Ning, Sci. Rep. **6**, 24996 (2016).
[28] A. Osterwalder, M. J. Nee, J. Zhou, and D. M. Neumark, J. Chem. Phys. **121**, 6317 (2004).
[29] D. M. Neumark, J. Phys. Chem. A **112**, 13287 (2008).
[30] J. B. Kim, J. A. DeVine, D. S. Levine, and D. M. Neumark, J. Am. Chem. Soc. **137**, 1420 (2015).
[31] J. B. Kim, M. L. Weichman, T. F. Sjorlander, D. M. Neumark, J. Klos, M. H. Alexander, and D. E. Manolopoulos, Science **349**, 510 (2015).
[32] I. Leon, Z. Yang, H. T. Liu, and L. S. Wang, Rev. Sci. Instrum. **85**, 083106 (2014).
[33] H. T. Liu, C. G. Ning, D. L. Huang, and L. S. Wang, Angew. Chem. Int. Ed. **52**, 8976 (2013).
[34] H. T. Liu, C. G. Ning, D. L. Huang, P. D. Dau, and L. S. Wang, Angew. Chem. Int. Ed. **53**, 2464 (2014).
[35] R. R. Corderman, P. C. Engelking, and W. C. Lineberger, J. Chem. Phys. **70**, 4474 (1979).
[36] D. G. Leopold and W. C. Lineberger, J. Chem. Phys. **85**, 51 (1986).
[37] L. A. Cole and J. P. Perdew, Phys. Rev. A **25**, 1265 (1982).
[38] N. B. Balabanov and K. A. Peterson, J. Chem. Phys. **123**, 064107 (2005).
[39] P. J. Mohr, D. B. Newell, and B. N. Taylor, arXiv:1507.07956.
[40] W. C. Wiley and I. H. Mclaren, Rev. Sci. Instrum. **26**, 1150 (1955).
[41] A. T. J. B. Eppink and D. H. Parker, Rev. Sci. Instrum. **68**, 3477 (1997).
[42] W. Li, S. D. Chambreau, S. A. Lahankar, and A. G. Suits, Rev. Sci. Instrum. **76**, 063106 (2005).
[43] B. Dick, Phys. Chem. Chem. Phys. **16**, 570 (2014).
[44] P. C. Engelking and W. C. Lineberger, Phys. Rev. A **19**, 149 (1979).
[45] J. C. Pickering and A. P. Thorne, Astrophys. J. Suppl. Ser. **107**, 761 (1996).
[46] R. J. Pelaez, C. Blondel, M. Vandevraye, C. Drag, and C. Delsart, J. Phys. B: At. Mol. Opt. Phys. **44**, 195009 (2011).
[47] A. E. Kramida, Comput. Phys. Commun. **182**, 419 (2011).